Journal of Mathematical Chemistry Vol. 27, No. 4, 2000

Evanescent energy in square and circular fibers

Gang Bao [a], Xiaohong Fang [b], Weihong Tan [b] and Tri Van [c]

[a] *Department of Mathematics, Michigan State University, East Lansing, MI 48824, USA*
E-mail: bao@math.msu.edu

[b] *Department of Chemistry, University of Florida, Gainesville, FL 32611, USA*
E-mail: {xfang; tan}@chem.ufl.edu

[c] *Air Force Institute of Technology, 2950 P.St., AFIT/ENC, WPAFB, OH 45433, USA*
E-mail: Tri.Van@afit.af.mil

Received 20 June 2000

A finite element method is presented to find the propagation characteristics of an optical fiber with arbitrary cross section. This method uses a non-local boundary operator to reduce the infinite problem (open waveguide) to a bounded one. Evanescent energy in circular and square fibers of the same core area are computed and compared to show that square fibers can be effectively used in single molecule detection.

KEY WORDS: evanescent energy, optical fibers, single-molecule detection, finite element method

1. Introduction

There has been a wide application of optical fibers in communication, medical equipment, remote measurement, and recently chemical and biochemical sensing. Taking the advantages of the evanescent field produced on the core surface of optical fibers, fiber optical evanescent wave sensors have the ability to give rapid and sensitive detection in real time. They are becoming important analytical tools and are attracting increasing interests [1]. Recently, we have found that the evanescent field generated by both circular silicon fiber and plastic square fiber can be used for the ultra-sensitive detection and imaging of single molecules [2]. We also noticed that the square fibers have some advantages over the circular fibers as they can provide a flat sensing area, which is very convenient for microscopic imaging [2]. Circular fibers are commonly used fibers and their evanescent fields have been well characterized [1,3]. Even though there are some studies on the propagation modes of a rectangular waveguide [4–7], the distribution of the evanescent field on a square fiber is unknown. A better understanding of the evanescent field should be very useful for the exploring of square fiber for sensing and other applications. Hence, the main effort of the paper is to gain more information on the evanescent field produced on a square fiber through numerical simulations.

In this paper, a variational method is developed to find the propagation characteristics (or propagation constants), hence, the evanescent energy, of an arbitrary optical fiber.

0259-9791/00/1200-0251$18.00/0

This method helps to reduce the computational effort to a bounded domain by coupling the solutions in the infinite homogeneous region to those in an inhomogeneous bounded region that contains the fiber core. Here, a fiber means that the cladding (i.e., the plastic cover) is removed and the core is exposed to directly interact with the surroundings.

The paper is arranged as follows. In section 2, we discuss the scalar wave equation (Helmholtz equation) for the electric field and the construction of the Dirichlet-to-Neumann boundary mapping. This mapping enables one to reduce the problem defined in an infinite domain to a problem in a bounded domain. In section 3, the variational formulation of the problem is given together with some of the theoretical results in error estimates which are proved in [8]. In section 4, a formula for computing the evanescent energy is presented. This formula is used in the last section (section 5) to study the evanescent energy outside of fibers. At the end of this section, a laboratory experiment of a square fiber used in detecting and imaging single molecules is included for completeness. For further details on the experiments, the reader is referred to the paper [2].

2. Problem setting

We consider an optical fiber with arbitrary cross section surrounded by a homogeneous medium. Let $\Omega \subset \mathbb{R}^2$ denote the fiber core. The fiber is characterized by the refractive-index profile, $n = n(x, y)$, which is assumed to be uniform in the fiber axis (or z-axis) and can be expressed as

$$n(x, y) = \begin{cases} f(x, y) & \text{in } \Omega, \\ n_{\mathrm{cl}} & \text{in } \mathbb{R}^2 \setminus \Omega, \end{cases}$$

where $f(x, y)$ is bounded and $n_{\mathrm{cl}} > 0$ is the cladding index (a constant). For wave guidance taking place in the fiber, it is assumed that $n_{\mathrm{cl}} < \max f(x, y)$ [3]. The scalar Helmholtz equation for the time-harmonic electric field is

$$\begin{cases} \Delta E + \left(k^2 n^2 - \beta^2\right) E = 0 & \text{in } \mathbb{R}^2, \\ \lim\limits_{r \to \infty} \sqrt{r} \left[\dfrac{\partial E}{\partial n} + \mathrm{i} k E \right] = 0 & \text{(radiation condition)}, \end{cases} \tag{2.1}$$

where $k = 2\pi/\lambda$ is the wave number, λ is the free space wavelength, and β is the propagation constant. This is an eigenvalue problem defined in the infinite domain $\mathbb{R}^2$ with β and E as eigenvalues and eigenfunctions, respectively. It is known that the propagation constant β of a propagating mode satisfies the condition [9]

$$k n_{\mathrm{cl}} < \beta \leqslant k \max f(x, y) \equiv k n_{\mathrm{co}}.$$

We assume that E and its normal derivative $\partial E/\partial n$ are continuous across the interfaces of different media. The infinite nature of the problem (2.1) poses a difficulty in finding β and E numerically for arbitrary core region Ω.

We now derive a variational formulation of the problem (2.1), which enables us to reduce the computational effort to a bounded domain. For this purpose, an artificial

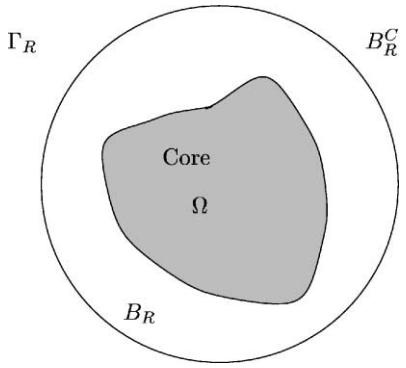

Figure 1. Computational domain B_R and artificial boundary Γ_R.

boundary is introduced so that the core of a fiber is completely contained in the bounded interior of the boundary. Here, we choose the circle Γ_R of radius $R > 0$. The exterior region $r > R$ is homogeneous, thus, analytical solutions are available. The region inside the circle, denoted by B_R, contains the core and a portion of the homogeneous medium (see figure 1). Thus, (2.1) can be rewritten as a transmission problem (P)

$$(P)\quad \begin{cases} \text{Find } kn_{\mathrm{cl}} < \beta < kn_{\mathrm{co}} \text{ and } E \in H^1(\mathbb{R}^2) \text{ such that} \\ \quad \Delta E^{\mathrm{i}} + \big(k^2 n^2(x,y) - \beta^2\big)E^{\mathrm{i}} = 0 \quad \text{in } B_R, \\ \quad \Delta E^{\mathrm{e}} + \big(k^2 n_{\mathrm{cl}}^2 - \beta^2\big)E^{\mathrm{e}} = 0 \quad \text{in } B_R^{\mathrm{c}} := \mathbb{R}^2 \setminus B_R, \\ \quad E^{\mathrm{i}} = E^{\mathrm{e}} \quad \text{on } \Gamma_R, \\ \quad \dfrac{\partial E^{\mathrm{i}}}{\partial n} = \dfrac{\partial E^{\mathrm{e}}}{\partial n} \quad \text{on } \Gamma_R, \\ \quad \lim\limits_{r\to\infty} \sqrt{r}\left[\dfrac{\partial E^{\mathrm{e}}}{\partial n} + \mathrm{i}\,kE^{\mathrm{e}}\right] = 0, \end{cases}$$

where $E^{\mathrm{i}} := E|_{B_R}$ and $E^{\mathrm{e}} = E|_{B_R^{\mathrm{c}}}$ are the restrictions of E and are called interior field and exterior field, respectively. In polar coordinates, the Helmholtz equation in B_R^{c} is transformed to

$$(P^{\mathrm{e}})\quad \begin{cases} \dfrac{\partial^2 E^{\mathrm{e}}}{\partial r^2} + \dfrac{1}{r}\dfrac{\partial E^{\mathrm{e}}}{\partial r} + \dfrac{1}{r^2}\dfrac{\partial^2 E^{\mathrm{e}}}{\partial \theta^2} - \big(\beta^2 - k^2 n_{\mathrm{cl}}^2\big)E^{\mathrm{e}} = 0, \\ \quad r > R,\ \theta \in [0, 2\pi], \\ E^{\mathrm{e}}(R,\theta) = E^{\mathrm{i}}(R,\theta), \\ \lim\limits_{r\to\infty} \sqrt{r}\left[\dfrac{\partial E^{\mathrm{e}}(r,\theta)}{\partial r} + \mathrm{i}\,kE^{\mathrm{e}}(r,\theta)\right] = 0. \end{cases} \tag{2.2}$$

An exterior solution E^{e} can be expressed as a Fourier series

$$E^{\mathrm{e}}(r,\theta) = \sum_{m=0}^{\infty} A_m \Phi_m(r) \begin{matrix} \cos(m\theta) & \text{(even mode)}, \\ \sin(m\theta) & \text{(odd mode)}, \end{matrix}$$

where A_m is a constant (to be determined) and $\Phi_m(r)$ satisfies the modified Bessel equations [10]

$$\frac{\mathrm{d}^2\Phi_m}{\mathrm{d}r^2} + \frac{1}{r}\frac{\mathrm{d}\Phi_m(r)}{\mathrm{d}r} - \left[\beta^2 - k^2 n_{\mathrm{cl}}^2 + \frac{m^2}{r^2}\right]\Phi_m(r) = 0, \quad m = 0, 1, 2, \ldots,$$
$$\lim_{r\to\infty} \sqrt{r}\left[\frac{\mathrm{d}\Phi_m}{\mathrm{d}r} + \mathrm{i}\,k\Phi_m\right] = 0,$$

where m is called the azimuthal mode number. Due to the radiation condition, the appropriate solutions of the modified Bessel equations are in terms of modified Bessel functions of the second kind

$$\Phi_m(r) = K_m(\alpha r), \quad m = 0, 1, 2, \ldots,$$

where $\alpha := \sqrt{\beta^2 - k^2 n_{\mathrm{cl}}^2} > 0$. Since $E^{\mathrm{e}} = E^{\mathrm{i}}$ on Γ_R, the coefficients A_m can be determined as

$$A_m = \frac{E^{\mathrm{i}(m)}}{K_m(\alpha R)},$$

where $E^{\mathrm{i}(m)}$ is the mth Fourier cosine (sine) coefficient of the interior solution E^{i}. Furthermore, the Neumann boundary condition $\partial E^{\mathrm{e}}/\partial n = \partial E^{\mathrm{i}}/\partial n$ on Γ_R yields the relation

$$\frac{\partial E^{\mathrm{i}}}{\partial n} = \frac{\partial E^{\mathrm{i}}}{\partial r}\bigg|_{r=R} = \sum \alpha \frac{E^{\mathrm{i}(m)}}{K_m(\alpha R)} K_m'(\alpha R) \begin{matrix}\cos(m\theta) & \text{(even mode)},\\ \sin(m\theta) & \text{(odd mode)}.\end{matrix}$$

One can easily see that the problem (P) is equivalent to [8]

$$(P^{\mathrm{i}}) \quad \begin{cases} \Delta E^{\mathrm{i}} + \left(k^2 n^2(x, y) - \beta^2\right) E^{\mathrm{i}} = 0 & \text{in } B_R, \\ \dfrac{\partial E^{\mathrm{i}}}{\partial n} = T_R\left(\beta; E^{\mathrm{i}}|_{\Gamma}\right) & \text{on } \Gamma_R, \end{cases}$$

where T_R is called the Dirichlet-to-Neumann mapping and is defined by

$$T_R(\beta; g) := \sum_{m=0}^{\infty} T_R^m(\beta; g) := \sum_{m=0}^{\infty} \alpha \frac{K_m'(\alpha R)}{K_m(\alpha R)} g^{(m)} \begin{matrix}\cos(m\theta),\\ \sin(m\theta),\end{matrix}$$

with $g^{(m)}$ is the mth Fourier cosine (sine) coefficients of a function g. The parameter β is included in the notation of T_R to emphasize the dependence of T_R on β through α. Thus, the infinite problem (P) is reduced to the bounded (interior) problem (P^{i}).

3. Variational formulation

In this section, we formulate the interior problem in a variational form. It is shown in [8] that the correct variational formulation of (P^{i}) is

$$(VP^{\mathrm{i}}) \quad \begin{cases} \text{Find } (\beta, u) \in (kn_{\mathrm{cl}}, kn_{\mathrm{co}}) \times H^1(B_R) \text{ such that} \\ \quad a(u, v) - m(\beta; u, v) = \lambda(\beta) b(u, v) \quad \forall v \in H^1(B_R), \end{cases}$$

where

$$a(u, v) := \int_{B_R} \left\{ \nabla u \cdot \nabla v + k^2 \left(n_\infty^2 - n^2(x, y) \right) uv \right\} \mathrm{d}x \, \mathrm{d}y,$$
$$m(\beta;\, u, v) := \oint_{\Gamma_R} T_R(\beta; u) v \, \mathrm{d}S,$$
$$b(\beta; u, v) := \int_{B_R} uv \, \mathrm{d}x \, \mathrm{d}y,$$
$$\lambda(\beta) := k^2 n_\infty^2 - \beta^2,$$

and $n_\infty > \max n(x, y)$ is an arbitrary constant and $H^1(B_R)$ is the usual Sobolev space. It is proved in [8] that the eigenvalues of the variational eigenvalue problem (VP^{i}) are isolated, which is important in the numerical viewpoint. We discretize (VP^{i}) by using a family of triangular meshes $\{\mathcal{T}_h\}$ where h is the longest side of all triangles in the triangulation $\mathcal{T}_h$ of B_R and by the linear polynomials in S_h^1 where

$$S_h^1 := \left\{ v_h \in H^1(B_R):\ v_h|_e \text{ is a linear polynomial},\ e \in \mathcal{T}_h \right\}.$$

Then the discrete analogue of (VP^{i}) is

$$(V_h P^{\mathrm{i}}) \quad \begin{cases} \text{Find } (\beta_h, u_h) \in (kn_{\mathrm{cl}}, kn_{\mathrm{co}}) \times S_h^1 \text{ such that} \\ \quad a(u_h, v_h) - m(\beta_h; u_h, v_h) = \lambda_h(\beta_h) b(u_h, v_h) \quad \forall v_h \in S_h^1. \end{cases}$$

We can rewrite the discrete problem ($V_h P^{\mathrm{i}}$) in the form of a non-linear eigenvalue matrix problem

$$\left[A - M(\beta) \right] U = \lambda(\beta) B U, \tag{3.1}$$

where A, $M(\beta)$ and B are the matrices corresponding to the bilinear forms $a(u, v)$, $m(\beta; u, v)$ and $b(u, v)$, respectively, and $\lambda(\beta) = k^2 n_\infty^2 - \beta^2$. Thus, we can view the eigenvalue (3.1) as a fixed-point problem

$$\lambda(\beta) - \left(k^2 n_\infty^2 - \beta^2 \right) = 0, \quad kn_{\mathrm{cl}} < \beta < kn_{\mathrm{co}},$$

which can be solved by applying the secant method. During the secant algorithm, one needs to solve the generalized linear eigenvalue problem

$$\begin{cases} \text{Given } \beta_0,\ \text{find } (\lambda, U) \text{ such that} \\ \quad \left[A - M(\beta_0) \right] U = \lambda B U. \end{cases} \tag{3.2}$$

This linear eigenvalue problem can be solved by any of the standard methods. In [8], optimal error estimates are established, that is, if (β, u) and (β_h, u_h) are eigensolutions of (VP^{i}) and ($V_h P^{\mathrm{i}}$), respectively, then

$$\|u - u_h\|_{H^1(B_R)} \leqslant C_1 h,$$
$$\|u - u_h\|_{L^2(B_R)} \leqslant C_2 h^2,$$

and

$$|\beta - \beta_h| \leqslant C_3 h^2,$$

where C_i $(i = 1, 2, 3)$ are positive constants independent of h.

Before ending this section, we briefly derive the exact eigenvalue equations for the step-index circular fiber with core radius a. The propagating fields in this type of optical fiber can be expressed analytically as

$$E(r, \theta, z) = \sum_{m=0}^{\infty} F_m(r)\Phi(\theta)\mathrm{e}^{-\mathrm{i}\beta_m z},$$

where each $F_m(r)$ is a solution of the Bessel's equation [10]

$$\left\{\frac{\mathrm{d}^2}{\mathrm{d}r^2} + \frac{1}{r}\frac{\mathrm{d}}{\mathrm{d}r} + \left(k^2 n^2(r) - \frac{m^2}{r^2}\right)\right\} F_m(r) = 0, \quad r \in (0, \infty),$$

with

$$n(r) = \begin{cases} n_{\mathrm{core}}, & 0 < r \leqslant a, \\ n_{\mathrm{cl}}, & r > a, \end{cases}$$

and $\Phi(\theta)$ is a solution of

$$\left(\frac{\mathrm{d}^2}{\mathrm{d}\theta^2} + m^2\right)\Phi(\theta) = 0, \quad \theta \in [0, 2\pi),$$

where m $(m = 0, 1, \ldots)$ is the azimuthal mode number. Since propagating fields are finite in the core and decay exponentially outside the core, we get

$$F_m(r) = \begin{cases} A_m J_m\left(\dfrac{U_m r}{a}\right) & \text{for } r \in [0, a], \\ B_m K_m\left(\dfrac{W_m r}{a}\right) & \text{for } r \in (a, \infty), \end{cases}$$

where J_m and K_m are Bessel functions and modified Bessel functions, respectively, and A_m, B_m are constants, and

$$U_m = a\sqrt{k^2 n_{\mathrm{core}} - \beta_m^2}, \qquad W_m = a\sqrt{\beta_m^2 - k^2 n_{\mathrm{cl}}}.$$

We normalize F_m at the core–cladding interface as

$$\widetilde{F}_m(r) = \begin{cases} \dfrac{J_m(U_m r/a)}{J_m(U_m)}, & 0 \leqslant r \leqslant a, \\ \dfrac{K_m(W_m r/a)}{K_m(W_m)}, & r > a. \end{cases}$$

By the continuity condition at the core–cladding interface, we obtain the following eigenvalue equations for the step-index circular fiber:

$$U_m \frac{J'_m(U_m)}{J_m(U_m)} = W_m \frac{K'_m(W_m)}{K_m(W_m)}, \quad m = 0, 1, 2, \ldots, \tag{3.3}$$

which can be solved numerically by Newton's method. It is conventional to denote the solutions to (3.3) as $\beta_{m,l}$ where $l = 1, 2, \ldots$.

4. Evanescent energy

We define the evanescent energy of the propagating field as the difference of the total energy and the core energy

$$\mathcal{E}_{\mathrm{e}} := \mathcal{E}_{\mathrm{total}} - \mathcal{E}_{\mathrm{core}},$$

where

$$\mathcal{E}_{\mathrm{core}} := \int_{\Omega} \left(|E|^2 + |\nabla E|^2\right) \mathrm{d}x\, \mathrm{d}y,$$
$$\mathcal{E}_{\mathrm{total}} := \int_{\mathbb{R}^2} \left(|E|^2 + |\nabla E|^2\right) \mathrm{d}x\, \mathrm{d}y.$$

The total energy can be computed by evaluating the integrals in

$$\mathcal{E}_{\mathrm{total}} = \int_{B_R} |E|^2 \,\mathrm{d}x\, \mathrm{d}y + \int_{B_R^c} |E|^2 \,\mathrm{d}x\, \mathrm{d}y + \int_{\mathbb{R}^2} |\nabla E|^2 \,\mathrm{d}x\, \mathrm{d}y. \tag{4.1}$$

The first integral on the right-hand side of (4.1) can be easily found from the finite element solution. For the second integral we use the exterior solution E^{e}

$$E^{\mathrm{e}}(r, \theta) = \sum_{m=0}^{\infty} E^{\mathrm{i}(m)} \frac{K_m(\alpha r)}{K_m(\alpha R)} \begin{matrix} \cos(m\theta), \\ \sin(m\theta), \end{matrix} \quad r > R,$$

where $E^{\mathrm{i}(m)}$ is the mth cosine (sine) coefficient of the interior field E^{i}. Using the following identity [10]:

$$\int K_m^2(az) z \,\mathrm{d}z = \frac{z^2}{2}\left[K_m^2(az) - K_{m+1}(az) K_{m-1}(az)\right],$$

we get

$$\int_{B_R^c} \left|E^{\mathrm{e}}\right|^2 \mathrm{d}x\, \mathrm{d}y = \int_0^{2\pi} \int_R^{\infty} \left|E^{\mathrm{e}}(r, \theta)\right|^2 r \,\mathrm{d}r\, \mathrm{d}\theta$$
$$= \pi R^2 \sum_{m=0}^{\infty} \frac{E^{\mathrm{i}(m)}}{K_m^2(\alpha R)}\left[K_{m+1}(\alpha R) K_{m-1}(\alpha R) - K_m^2(\alpha R)\right].$$

Finally, since $E = E^{\mathrm{i}} + E^{\mathrm{e}}$ is the a solution of the Helmholtz equation in $\mathbb{R}^2$, the last integral on the right-hand side of (4.1) can be computed by

$$\begin{aligned}\int_{\mathbb{R}^2} |\nabla E|^2 \,\mathrm{d}x\,\mathrm{d}y &= \int_{\mathbb{R}^2} \left(k^2 n^2 - \beta^2\right)|E|^2 \,\mathrm{d}x\,\mathrm{d}y \\ &= \int_{B_R} \left(k^2 n^2 - \beta^2\right)\left|E^{\mathrm{i}}\right|^2 \mathrm{d}x\,\mathrm{d}y + \left(k^2 n_{\mathrm{cl}}^2 - \beta^2\right)\int_{B_R^{\mathrm{c}}} \left|E^{\mathrm{e}}\right|^2 \mathrm{d}x\,\mathrm{d}y.\end{aligned}$$

5. Computational results

This section is devoted to the computation of the eigenvalues and eigenvectors of (P^{i}) using the finite element method discussed in section 3. The dimension of the circular fiber and the square fiber is specified by its radius and half of its diameter (i.e., half of its diagonal), respectively. In each case, the artificial boundary is chosen to be the concentric circle of radius twice the fiber dimension. For example, if the radius of the circular fiber is a then the artificial boundary is the concentric circle of radius $2a$, and similarly, if the diameter of the square fiber is d then the artificial boundary circle is of radius d. For convenience, we always scale the problems so that the artificial boundary is of radius 2 (dimensionless). More precisely, the problem (P^{i}) is transformed to

$$\begin{cases} \Delta E^{\mathrm{i}} + \left(a^2 k^2 n^2 - \beta^2\right) E^{\mathrm{i}} = 0 & \text{in } B_2, \\ \dfrac{\partial E^{\mathrm{i}}}{\partial n} = T_2\left(\beta;\, E^{\mathrm{i}}|_{\Gamma_2}\right) & \text{on } \Gamma_2, \end{cases}$$

where

$$T_2(\beta;\, g) := \sum_{m=0}^{\infty} T_2^m(\beta;\, g) := \sum_{m=0}^{\infty} \alpha \frac{K_m'(2\alpha)}{K_m(2\alpha)} g^{(m)} \begin{matrix}\cos(m\theta), \\ \sin(m\theta),\end{matrix}$$

and

$$\alpha = \begin{cases} \sqrt{\beta^2 - a^2 k^2 n_{\mathrm{cl}}^2} & \text{for the circular fiber,} \\ \sqrt{\beta^2 - (d/2)^2 k^2 n_{\mathrm{cl}}^2} & \text{for the square fiber.} \end{cases}$$

Thus, we do simulations for "scaled" fibers of radius 1 and of diameter 2.

We first demonstrate the accuracy of the finite element method. Consider the circular fiber of radius 1 whose core index is $n_{\mathrm{co}} = 1.49$ and the cladding index is $n_{\mathrm{cl}} = 1.33$. The operating wavelength is $\lambda = 0.514$. In table 1, some of the largest eigenvalues are computed by the finite element method (FEM) and compared to those found by the exact eigenvalue equations (3.3). We see that the FEM eigenvalues are very accurate for a medium size mesh. In appendix, the intensity plots of the eigenfunctions (propagating modes) are given.

Next, we consider the plastic square fiber with the same core area as the circular fiber, i.e., the core index is $n_{\mathrm{co}} = 1.49$ and the diameter is $2\sqrt{\pi/2}$. The percentage of evanescent energy $\mathcal{E}_{\mathrm{e}}$ existing outside the core of each fiber for first four propagating

Table 1
Accuracy of the variational method. Circular fiber of radius $a = 1$, wavelength $\lambda = 0.514$, core index $n_{\mathrm{co}} = 1.49$, cladding index $n_{\mathrm{cl}} = 1.33$.

FEM eigenvalues (vertices = 169)	FEM eigenvalues (vertices = 625)	FEM eigenvalues (vertices = 2401)	Exact eigenvalues ($\beta_{m,l}$)
18.0782	18.0853	18.0871	18.0876 ($m = 0, l = 1$ – mode 1)
17.8513	17.8827	17.8903	17.8928 ($m = 1, l = 1$ – mode 2)
17.5365	17.6112	17.6295	17.6356 ($m = 2, l = 1$ – mode 3)
17.4951	17.5136	17.5388	17.5472 ($m = 0, l = 2$ – mode 4)
17.0562	17.2543	17.3024	17.3182 ($m = 3, l = 1$ – mode 5)
16.8505	17.0644	17.1195	17.1378 ($m = 1, l = 2$ – mode 6)
16.5117	16.5337	16.5599	16.5979 ($m = 0, l = 3$ – mode 7)

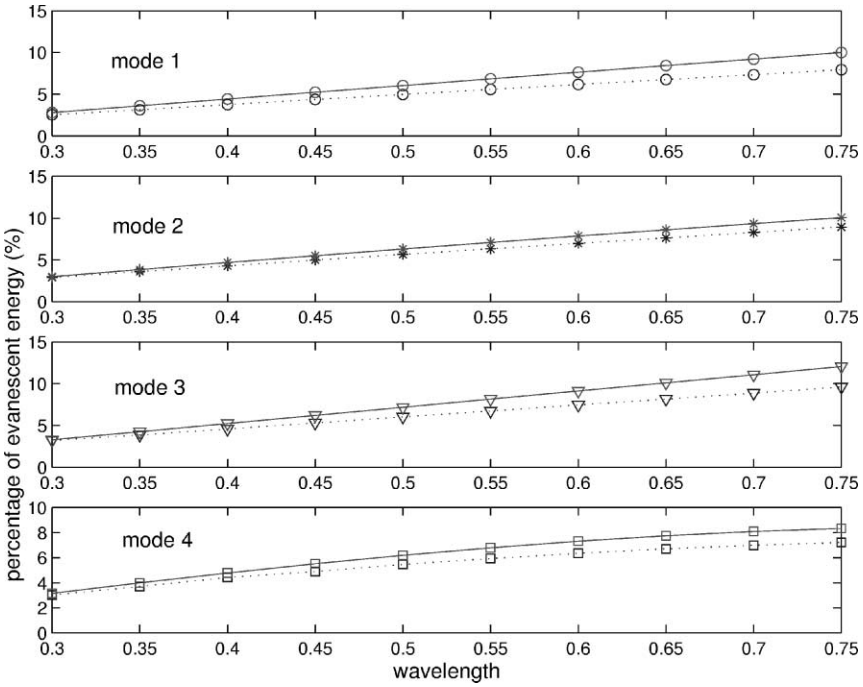

Figure 2. $\mathcal{E}_{\mathrm{e}}$ (%) versus λ. (—): square fiber of diameter $d = 2\sqrt{\pi/2}$. $(\cdots)$: circular fiber of radius $a = 1$. Core index $n_{\mathrm{co}} = 1.49$. Cladding index $n_{\mathrm{cl}} = 1.33$.

modes is computed as a function of wavelength ($0.3 \leqslant \lambda \leqslant 0.8$) and cladding index ($1.33 \leqslant n_{\mathrm{cl}} \leqslant 1.42$). This is sufficient since these modes are known to have highest energy [11]. We observe that the square fiber yields slightly more evanescent energy than the corresponding circular fiber for each considered propagating mode (see figures 2 and 3). It is worth noting that in practice, the dimension of fibers and wavelengths always appear in ratio: dimension/wavelength. Thus, the behavior of evanescent energy as the fiber dimension varies is equivalent to that as the wavelength varies. In appendix, the

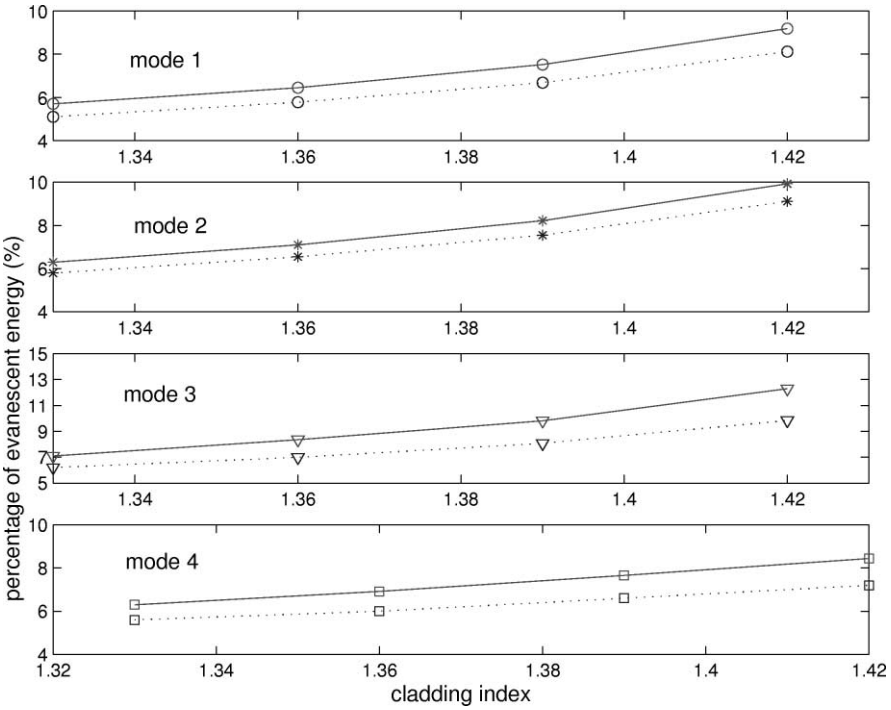

Figure 3. $\mathcal{E}_e$ (%) versus n_{cl}. (—): square fiber of diameter $d = 2\sqrt{\pi/2}$. $(\cdots)$: circular fiber of radius $a = 1$. Core index $n_{co} = 1.49$. Cladding index $n_{cl} = 1.33$.

intensity plots of the propagating modes in the square fiber are given for $\lambda = 0.514$ and $n_{cl} = 1.33$.

Finally, we present an example of using polymethylmethacrylate (PMMA) plastic square fiber (core index $n_{co} = 1.49$) to detect and image single molecules. The fiber with 1 mm = 1000 μm width core was cut to about 30 cm long. At one end of the fiber, the cladding was mechanically peeled off to expose a 4 cm long core area. This end was inserted into a channel which was placed on the stage of a microscope and filled with a fluorescent dye sample solution. A laser beam was directed to the other end of the fiber. Evanescent field was generated on the core surface of the fiber and was used to excite the flurophores in the solution. Fluorescent signals thus produced by the molecules close the fiber surface were collected by a microscope objective and then directed to an intensified charge coupled device (ICCD) to get the images as shown in figure 4. Considering the depth of the evanescent field ($\approx$ 200 nm) and the size of each pixel ($0.23 \times 0.23 \mu m^2$) in the ICCD, one pixel of the ICCD only detects a volume which is small enough to isolate individual molecules with fluorophore concentration used in the experiment [2]. The image obtained for water (see figure 4(A)) was used to determine the threshold for single R6G images. Therefore, each bright spot in figure 4(B) corresponds to the fluorescent signal from a single R6G molecule.

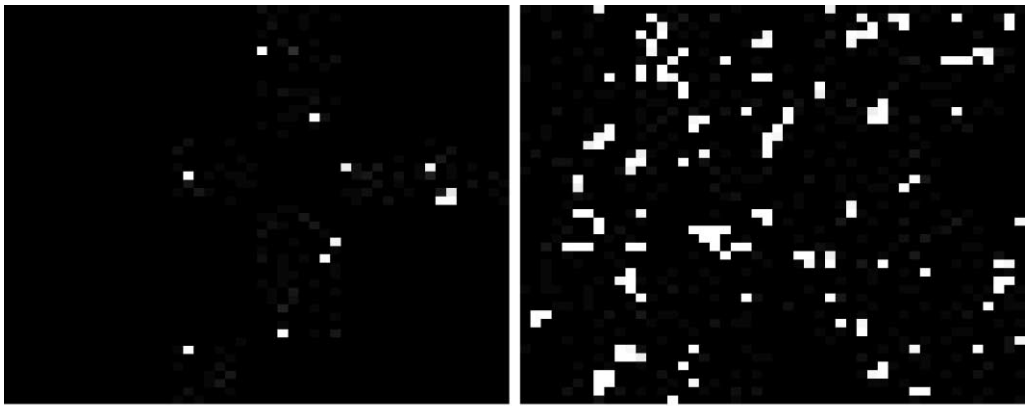

Figure 4. Fluorescent image (50×50 pixel subframe image) obtained from single R6G molecules in water by 1 mm core square fiber probe. A: purified water. B: 1.7×10^{-8} M. R6G molecules are excited at 514 nm and their fluorescent signals were collected through a 550 nm band pass filter.

Acknowledgements

The research of G. Bao and T. Van was partially supported by the NSF grant DMS 98-03604, the NSF University–Industry Cooperative Research Programs grants DMS 98-03809, DMS 99-72292, and the NSF Western Europe Programs grant INT 98-15798. The research of X. Fang and W. Tan was supported by NSF Faculty Career Award CHE-9733650 and by Office of Naval Research Young Investigator Award N00014-98-1-0621. We thank Dr. Peng Zhang for helpful discussion.

Appendix

For each propagating mode E, we define its normalized total intensity I and normalized exterior intensity I_{e} as

$$I = \frac{|E|^2}{\max |E|^2}, \qquad I_{\mathrm{e}} = \frac{|E^{\mathrm{e}}|^2}{\max |E|^2}.$$

The following are the intensity plots of propagating modes in the circular and square fibers:

- *Circular fiber*: $a = 1$, $n_{\mathrm{co}} = 1.49$, $n_{\mathrm{cl}} = 1.33$, and $\lambda = 0.514$. See figures 5–9.
- *Square fiber*: diameter $d = 2\sqrt{\pi/2}$, $n_{\mathrm{co}} = 1.49$, $n_{\mathrm{cl}} = 1.33$, $\lambda = 0.514$. See figures 10–14.

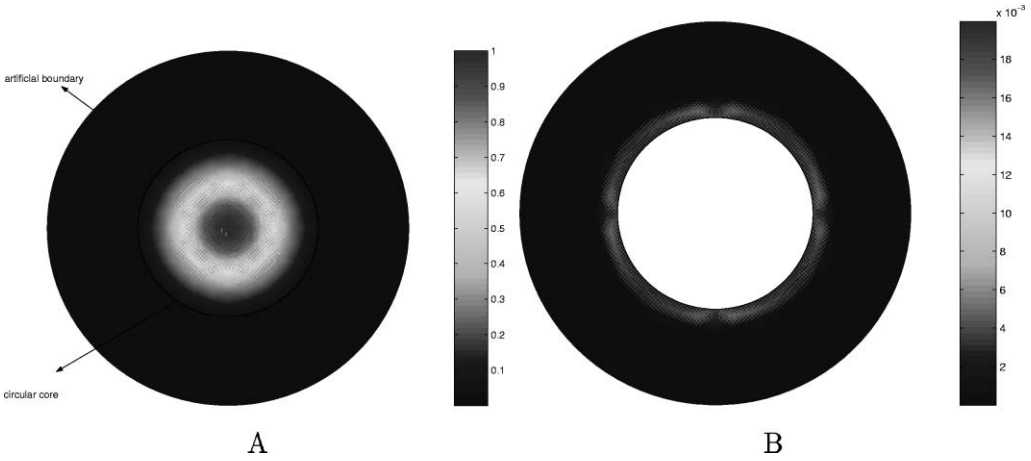

Figure 5. Mode 1 (fundamental mode). A: normalized total intensity I. B: cladding intensity I_e.

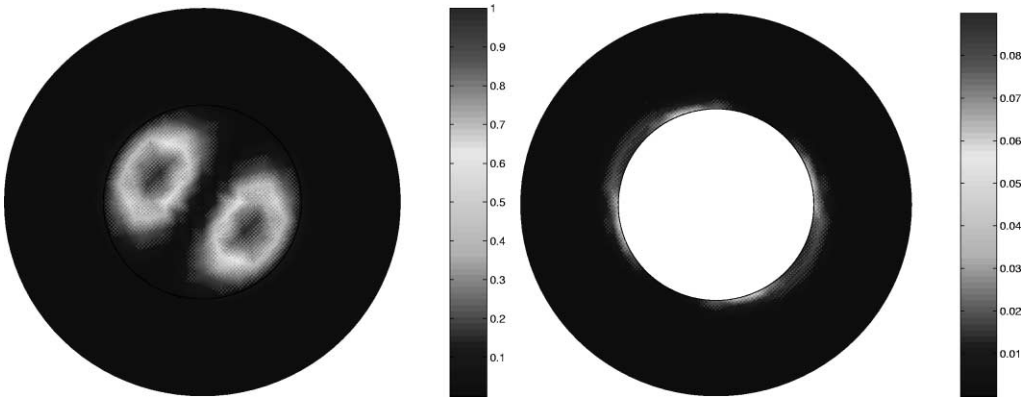

Figure 6. Mode 2. The eigenvalue for this mode has multiplicity 2. Thus, the other mode is obtained by a $\pi/2$-rotation.

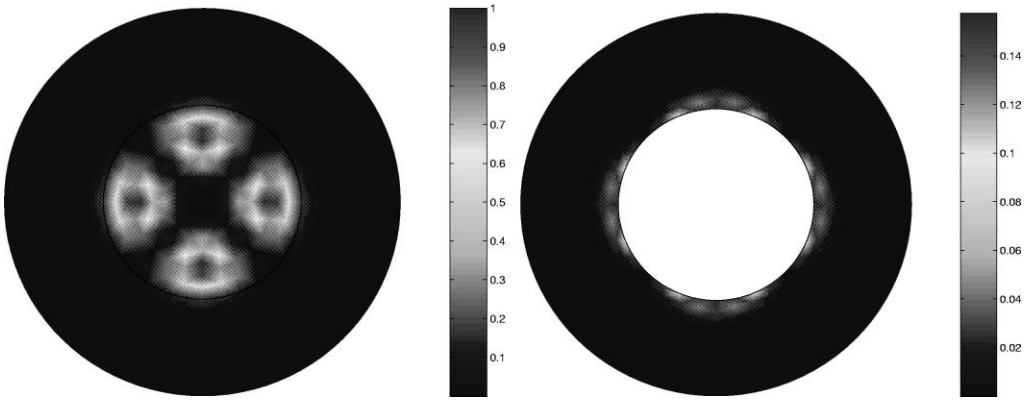

Figure 7. Mode 3. The eigenvalue for this mode has multiplicity 2. Thus, the other mode is obtained by a $\pi/4$-rotation.

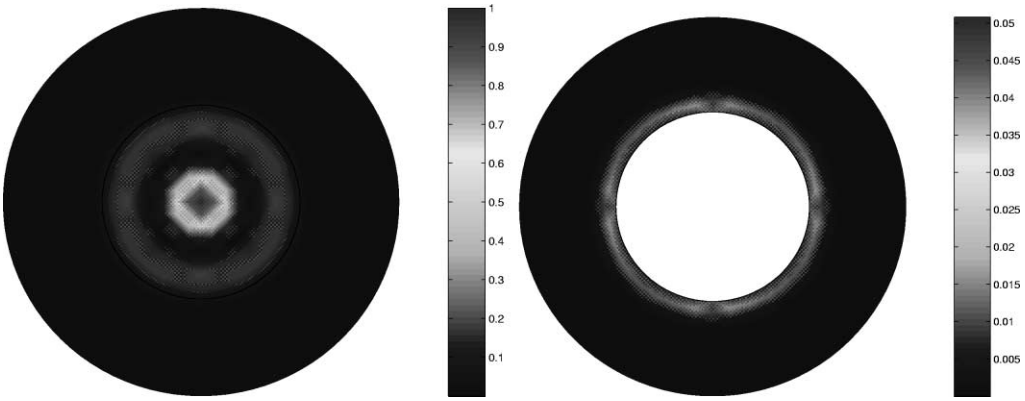

Figure 8. Mode 4.

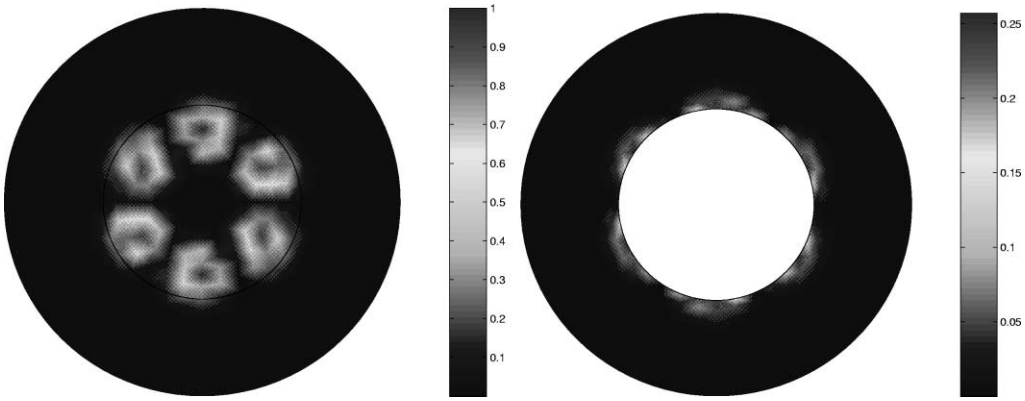

Figure 9. Mode 5. The eigenvalue for this mode has multiplicity 2. Thus, the other mode is obtained by a $\pi/4$-rotation.

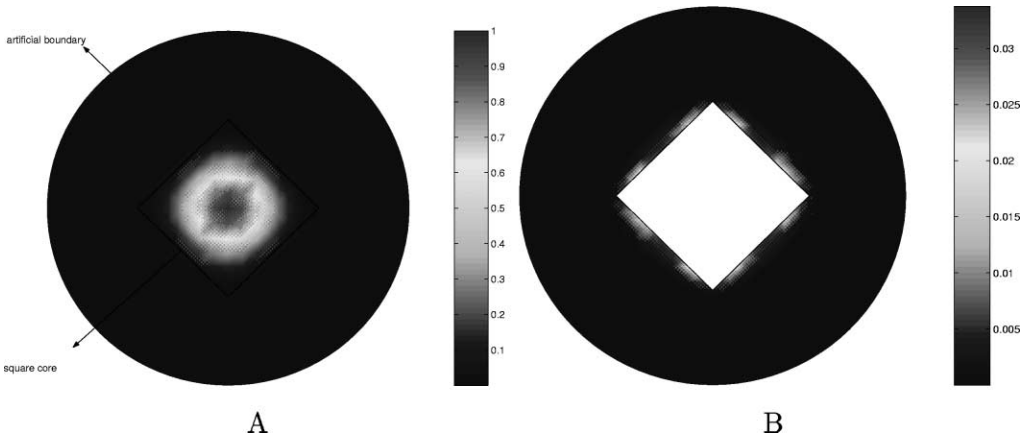

Figure 10. Mode 1 (fundamental mode). A: normalized total intensity I. B: cladding intensity I_e.

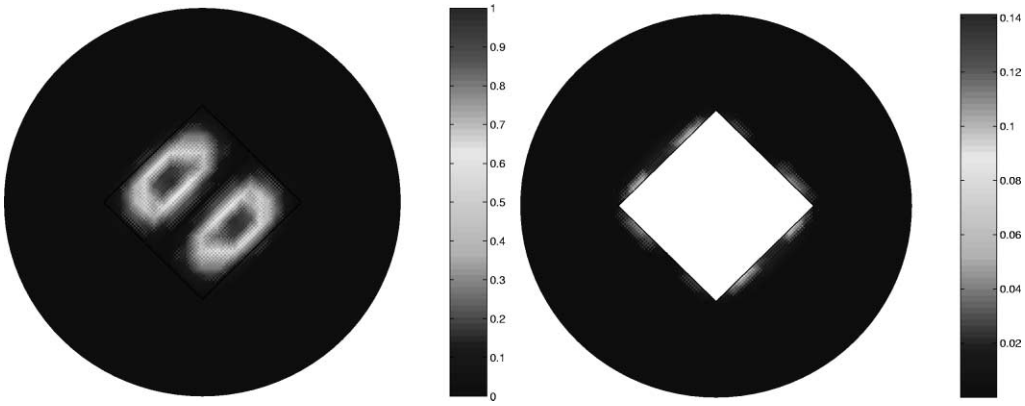

Figure 11. Mode 2. The eigenvalue for this mode has multiplicity 2. Thus, the other mode is obtained by a $\pi/2$-rotation.

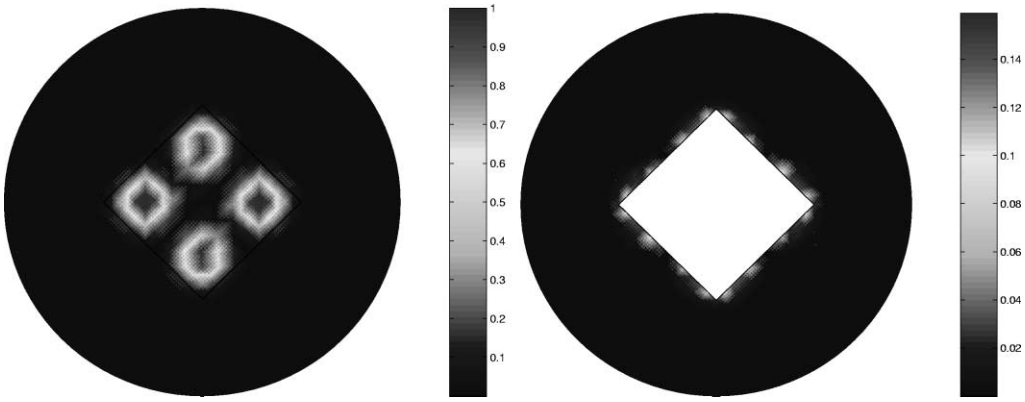

Figure 12. Mode 3. The eigenvalue for this mode has multiplicity 2. Thus, the other mode is obtained by a $\pi/2$-rotation.

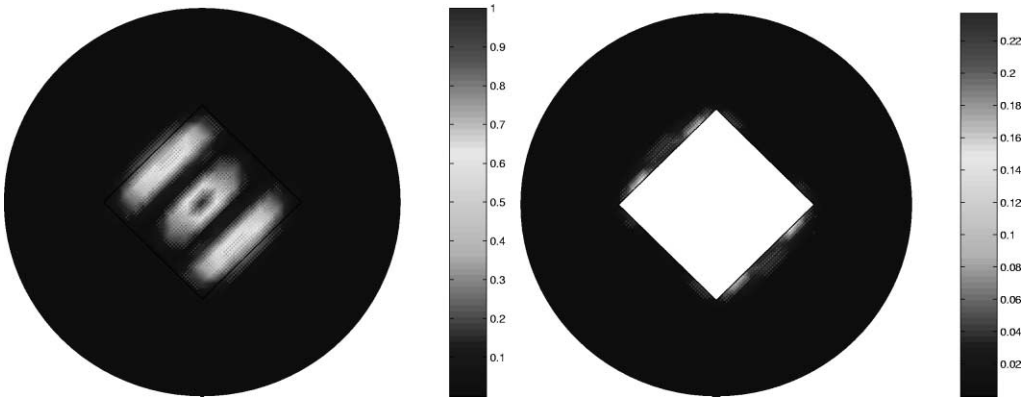

Figure 13. Mode 4. The eigenvalue for this mode has multiplicity 2. Thus, the other mode is obtained by a $\pi/2$-rotation.

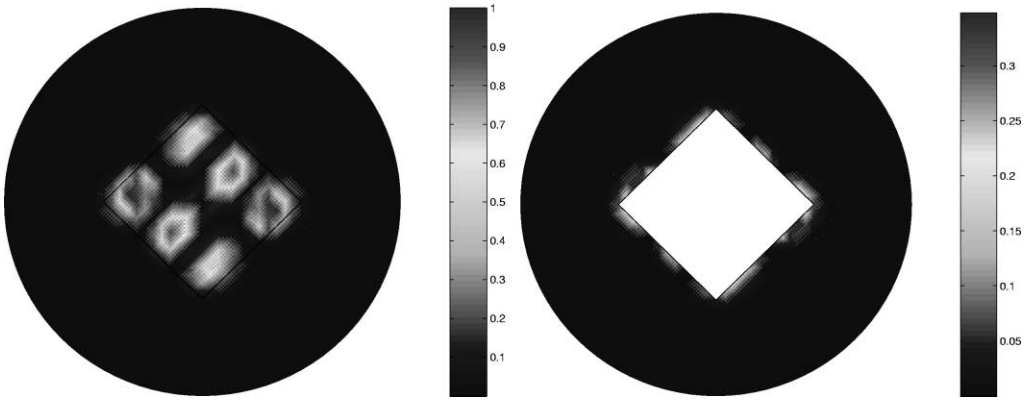

Figure 14. Mode 5. The eigenvalue for this mode has multiplicity 2. Thus, the other mode is obtained by a $\pi/2$-rotation.

References

[1] W. Love, L. Button and R. Slovacek, Optical characteristics of fiberoptics evanescent wave sensor, in: *Biosensors with Fiber Optics*, eds. D.L. Wise and L.B. Wingard, Jr. (The Humana Press, 1991).
[2] X. Fang and W. Tan, Imaging single fluorescent molecules at the interface of an optical fiber probe by evanescent wave excitation, Anal. Chem. 71 (1999) 3101–3105.
[3] A.W. Snyder and J.D. Love, *Optical Waveguide Theory* (Chapman-Hall, London, 1983).
[4] R.E. Collin, *Field Theory of Guided Wave*, 2nd ed. (IEEE Press, 1991).
[5] J.E. Goell, A circular-harmonic computer analysis of rectangular dielectric waveguides, The Bell System Technical Journal (1969) 2133–2160.
[6] E.A.J. Marcatili, Dielectric rectangular waveguide and directional coupler for integrated optics, The Bell System Technical Journal (1969) 2071–2102.
[7] T. Tamir (ed.), *Guided-wave Optoelectronics*, 2nd ed. (Springer-Verlag, Berlin, 1990).
[8] G. Bao and T. Van, Modeling of evanescent energy in optical fibers, J. Comput. Phys. (to appear).
[9] D. Marcuse, *Theory of Dielectric Optical Waveguides* (Academic Press, New York, 1974).
[10] M. Abramowitz and I. Stegun, *Handbook of Mathematical Functions with Formulas, Graphs, and Mathematical Tables* (Dover, New York, 1972).
[11] A.W. Snyder, Excitation and scattering of modes on a dielectric or optical fiber, IEEE Trans. Microwave Theory and Techniques 17 (1969) 1138–1144.